Geosci. Model Dev. Discuss., 8, 9965–10009, 2015
www.geosci-model-dev-discuss.net/8/9965/2015/
doi:10.5194/gmdd-8-9965-2015

Geoscientific Model Development Discussions
Open Access
EGU

Impacts of air–sea interactions on regional air quality predictions using WRF/Chem v3.6.1 coupled with ROMS v3.7: southeastern US example

J. He, R. He, and Y. Zhang

Department of Marine, Earth, and Atmospheric Sciences, North Carolina State University, Raleigh, NC, USA

Received: 17 September 2015 – Accepted: 20 October 2015 – Published: 13 November 2015

Correspondence to: Y. Zhang (yang_zhang@ncsu.edu)

Published by Copernicus Publications on behalf of the European Geosciences Union.

Abstract

Air–sea interactions have significant impacts on coastal convection and surface fluxes exchange, which are important for the spatial and vertical distributions of air pollutants that affect public health, particularly in densely populated coastal areas. To understand the impacts of air–sea interactions on coastal air quality predictions, sensitivity simulations with different cumulus parameterization schemes and atmosphere–ocean coupling are conducted in this work over southeastern US in July 2010 using the Weather Research and Forecasting Model with Chemistry (WRF/Chem). The results show that different cumulus parameterization schemes can result in an 85 m difference in the domain averaged planetary boundary layer height (PBLH), and 4.8 mm difference in the domain averaged daily precipitation. Comparing to WRF/Chem without air–sea interactions, WRF/Chem with a 1-D ocean mixed layer model (WRF/Chem-OML) and WRF/Chem coupled with a 3-D Regional Ocean Modeling System (WRF/Chem-ROMS) predict the domain averaged changes in the sea surface temperature of 0.1 and 1.0 °C, respectively. The simulated differences in the surface concentrations of ozone (O_3) and $PM_{2.5}$ between WRF/Chem-ROMS and WRF/Chem can be as large as 17.3 ppb and 7.9 μg m^{-3}, respectively. The largest changes simulated from WRF/Chem-ROMS in surface concentrations of O_3 and particulate matter with diameter less than and equal to 2.5 μm ($PM_{2.5}$) occur not only along coast and remote ocean, but also over some inland areas. Extensive validations against observations, show that WRF/Chem-ROMS improves the predictions of most cloud and radiative variables, and surface concentrations of some chemical species such as sulfur dioxide, nitric acid, maximum 1 h and 8 h O_3, sulfate, ammonium, nitrate, and particulate matter with diameter less than and equal to 10 μm (PM_{10}). This illustrates the benefits and needs of using coupled atmospheric–ocean model with advanced model representations of air–sea interactions for regional air quality modeling.

GMDD
8, 9965–10009, 2015

1 Introduction

3-D regional atmospheric models, such as the Weather Research and Forecasting model with chemistry (WRF/Chem, Grell et al., 2005; Fast et al., 2006; Zhang et al., 2010), the Community Multi-scale Air Quality (CMAQ, Binkowski and Roselle, 2003; Byun and Schere, 2006) model, and the Comprehensive Air Quality Model with Extensions (CAMx, ENVIRON, 1998, 2010), are often used for regional air quality studies at high resolutions of 4–36 km. Most regional models consist of an atmospheric component coupled to a land surface scheme and forced by prescribed sea surface temperature (SST) over ocean. However, SST patterns can impact precipitation patterns and therefore affect atmospheric heating through latent heat flux. As a result, boundary layer conditions are impacted through air–sea interactions, resulting in changes in the planetary boundary height (PBLH), surface temperature, and surface wind. Most coastal areas contain dense population. The air pollutants such as ozone (O_3) and particulate matter (PM) trapped in the boundary layer of these regions can have adverse impacts on human health and environment. The changes in the horizontal SST gradients can impact the surface fluxes at atmosphere–ocean interface, which leads to changes in convection and PBLH. Both have significant impacts on temporal and spatial distribution of dust, sea-salt emissions and chemical species that in turn affect human health, environment, and ecology. As such, it is also important to include the representations of air–sea interactions in regional air quality studies.

Modeling air–sea interaction process is an active field of research in oceanography. For example, Warner et al. (2010) reported the Coupled Ocean–Atmosphere–Wave–Sediment Transport (COAWST) Modeling System, which couples the atmosphere model WRF (http://www2.mmm.ucar.edu/wrf/users/docs/user_guide_V3/ARWUsersGuideV3.pdf), with the Regional Ocean Modeling System (ROMS, Shchepetkin et al., 2005) (hereafter WRF-ROMS). The coupling system has been applied for a number of regional air–sea interaction studies (Nelson and He, 2012; Nelson et al.,

GMDD
8, 9965–10009, 2015

2014; Zambon et al., 2014a, b), focused on the effects of air–sea interactions on atmospheric dynamics and ocean circulation.

Meteorology and radiation are important for distribution and concentration of air pollutants (e.g., transport of air pollutants, photolysis, and chemical reactions). On the other hand, chemical species can influence the meteorological and cloud/radiative variables by perturbing the atmospheric radiation budget and through cloud properties. While many of these coupled modeling systems include prescribed or constant chemistry (e.g., prescribed O_3 or AOD), little work has been done using coupled regional air quality and regional ocean model. In this work, building on existing coupled WRF-ROMS in COAWST version 3.1, WRF/Chem version 3.6.1 is coupled with ROMS version 3.7 (hereafter WRF/Chem-ROMS) in COAWST to study the effects of air–sea interactions on regional air quality. The major objective in this work is to examine the impacts of air–sea interactions on model predictions of meteorology, chemistry, and cloud/radiation over coastal regions.

2 Model configurations and evaluation protocols

2.1 Model description and setup

The WRF/Chem model is used in this work to represent the atmospheric conditions. It is based on WRF/Chem version 3.6.1 with additional modifications and updates by Wang et al. (2015a). The major updates include (1) the coupling of the 2005 Carbon Bond (CB05) gas-phase (Yarwood et al., 2005; Sarwar et al., 2008) with the existing Modal of Aerosol Dynamics in Europe with the Volatility Basis Set (MADE-VBS, Grell et al., 2005; Ahmadov et al., 2012) approach for simulating secondary organic aerosol (SOA); (2) incorporating the aqueous chemistry (AQChem) module of CMAQ version 5.0 (Sarwar et al., 2011) into WRF/Chem. This new chemistry-aerosol option of CB05-MADE/VBS has been coupled with existing model treatments and has been demonstrated its capability to simulate chemistry–aerosol–radiation–cloud feedbacks

GMDD
8, 9965–10009, 2015

such as aerosol semi-direct effects on photolysis rates of major gases, aerosol indirect effects on cloud droplet numbers, and cloud effects on shortwave radiation (Wang et al., 2014a, b; Yahya et al., 2014, 2015). In this work, this chemistry-aerosol option of CB05-MADE/VBS is applied for all the WRF/Chem simulations.

Table 1 shows the simulations conducted in this work. The WRF/Chem simulations are conducted over southeastern US for July 2010, with 12 km horizontal resolution (i.e., 160 × 210 grid cells) and a vertical resolution of 35 layers from the surface to 100 hPa, with a surface layer model height of 38 m. The emissions for WRF/Chem are from Wang et al. (2015b), which is based on the 2008 National Emission Inventory (NEI) (version 2, released 10 April 2012). The meteorological initial and boundary conditions (ICs and BCs) are generated from the National Center for Environmental Prediction Final Analysis (NCEP-FNL) and the chemical ICs and BCs are from the Community Earth System Model (CESM) every 6 h output (He et al., 2015). The physics options used for baseline simulation (BASE) is summarized in Table 1 of Wang et al. (2015a). The cumulus parameterization scheme used in this work is based on Grell 3D ensemble scheme (referred to as G3D, Grell and Freitas, 2014), which allows for a series of different assumptions that are commonly used in convective parameterizations and includes options to spread subsidence to neighboring grid points. Besides for the options listed in Table 1 of Wang et al. (2015a), BASE also includes prescribed SST forcing from NCEP by updating every 6 h. SEN1 is conducted with the same model configurations as BASE but with different cumulus parameterization scheme based on Grell and Freitas (2014) (referred to as GF scheme), which allows for subgrid scale convection representation. The differences in the model results between BASE and SEN1 can provide insights about the sensitivity of cumulus parameterization on model meteorological, cloud/radiative, and chemical predictions.

SEN2 is configured same as SEN1 but with 1-dimentional (1-D) ocean mixed layer (OML) model turned on (hereafter WRF/Chem-OML). A simple OML module based on Pollard et al. (1973) is available in WRF/Chem, which includes wind-driven ocean mixing and mixed layer deepening process. Surface wind stress generates currents

GMDD
8, 9965–10009, 2015

in the ocean mixed layer (typically 30–100 m deep), which leads to mixing with cooler water below. The model does not consider pressure gradients or horizontal advection, but does include Coriolis, which is important for the rotation of inertial currents and SST cooling. This process deepens and cools the mixed layer, which changes SST and hence surface fluxes. The initial mixed layer depth (i.e., 50 m) and temperature lapse rate (i.e., 0.14 $K m^{-1}$) are specified in the model for the entire domain, which is a significant source of uncertainty considering spatial variations. The OML model is called every model time step (i.e., 60 s) across every grid point and the SST is then fed back into the atmospheric model (i.e., WRF/Chem).

SEN3 has the same WRF/Chem configuration as SEN1, but with fully coupling with ROMS (updated through August 2014) (i.e., WRF/Chem-ROMS). ROMS is a 3-dimentional (3-D), free-surface, hydrostatic, and primitive equations ocean model, which uses vertically stretched terrain-following (σ) coordinates combined with advanced physics packages to allow simulation of advective processes, Coriolis, and viscosity in 3-dimensions. It includes high-order advection and time-stepping schemes, weighted temporal averaging of the barotropic mode, conservative parabolic splines for vertical discretization, and the barotropic pressure gradient term, which can be applied for estuarine, coastal and basin-scale oceanic processes (Marchesiello et al., 2003; He and Wilkin, 2006; He et al., 2008). The COAWST (Warner et al., 2010) modeling system is designed to enable the integration of oceanic, atmospheric, wave, and morphological processes in the coastal ocean. It consists of three state-of-the-art numerical models representing the atmosphere (i.e., WRF), ocean (i.e., ROMS) and wave (i.e., Simulating WAves Nearshore, SWAN) conditions using the Model Coupling Toolkit (MCT). COAWST represents the frontier in regional air–sea interaction modeling.

In this work, COAWST is configured for a two-way coupling only between WRF and ROMS. NCSU's version of WRF/Chem replaces WRF and is coupled with ROMS within COAWST system to provide insights about effects of air–sea interactions on coastal air quality. ROMS is configured on the same grid resolution as WRF/Chem with 157 interior density (ρ) points in the Y direction and 207 interior ρ points in the X direction, and

GMDD
8, 9965–10009, 2015

with 16 layers vertically in the ocean. The initial and boundary conditions are from the global HYbrid Coordinate Ocean Model (HYCOM) combined with the Navy Coupled Ocean Data Assimilation (NCODA) (http://tds.hycom.org/thredds/catalog.html). The coastline and bathymetry are extracted from the Global Self-consistent Hierarchical High-resolution Shorelines (GSHHS), and 5-Minute Gridded Global Relief Data Collection (ETOPO5), respectively. Figure 1 shows the diagram of the coupling WRF/Chem with ROMS within the COAWST framework. ROMS is coupled with WRF through MCT. SST is computed inside ROMS and then passed to WRF/Chem. Meanwhile, several variables are passed from WRF/Chem to ROMS, including net heat flux and wind stress. The time step for ROMS calculation is 30 s and the time frequency for the WRF/Chem-ROMS coupling is 10 min. The simulations are conducted for entire July 2010, with 7 days (24–30 June 2014) for spinup. The model output frequency is hourly.

2.2 Available measurements and evaluation protocols

A number of observational datasets from surface networks and satellites are used for model evaluation. They are summarized along with the variables to be evaluated in Table 2. The meteorological and radiative variables are evaluated, including temperature at 2 m (T2), relative humidity at 2 m (RH2), and wind speed at 10 m (WS10) observed from the National Climatic Data Center (NCDC, ftp://ftp.ncdc.noaa.gov/pub/data/noaa); daily precipitation rate (Precip) derived from the Global Precipitation Climatology Project (GPCP, http://www.esrl.noaa.gov/psd/data/gridded/data.gpcp.html) and the Multi-satellite Precipitation Analysis from the Tropical Rainfall Measuring Mission (TMAP, http://disc.sci.gsfc.nasa.gov/gesNews/trmm_v7_multisat_precip); outgoing longwave radiation (OLR), downwelling shortwave radiation (SWD), downwelling longwave radiation (LWD), shortwave cloud forcing (SWCF), and longwave cloud forcing (LWCF) retrieved from the Clouds and Earth's Radiant Energy System (CERES) Energy Balanced And Filled data product (CERES-EBAF, http://ceres.larc.nasa.gov/compare_products.php); cloud fraction (CF), cloud optical thickness (COT), and cloud

GMDD
8, 9965–10009, 2015

liquid water path (LWP) retrieved from the CERES Synoptic product at 1° spatial resolution (CERES-SYN1deg, http://ceres.larc.nasa.gov/compare_products.php); aerosol optical depth (AOD), precipitating water vapor (PWV), and cloud condensation nuclei at supersaturation of 0.5 % (CCN5) retrieved from the Moderate Resolution Imaging Spectroradiometer (MODIS, https://ladsweb.nascom.nasa.gov/data/search.html). Air–sea interaction related variables are evaluated including SST and WS10 from the National Data Buoy Center (NDBC, http://www.ndbc.noaa.gov/); PBLH derived from the National Centers for Environmental Prediction (NCEP)/North American Regional Reanalysis (NARR, http://www.esrl.noaa.gov/psd/data/gridded/data.narr.html); SST, sensible heat flux (SHFLX) and latent heat flux (LHFLX) derived from the Objectively Analyzed Air–Sea Fluxes (OAFlux, http://oaflux.whoi.edu/dataproducts.html). Surface chemical concentrations evaluated include O_3, sulfur dioxide (SO_2), nitric acid (HNO_3), particulate matter with diameter less and equal to 2.5 µm ($PM_{2.5}$) and 10 µm (PM_{10}), and $PM_{2.5}$ components such as sulfate (SO_4^{2-}), ammonium (NH_4^+), nitrate (NO_3^-), sodium (Na^+), chloride (Cl^-), elementary carbon (EC), and organic carbon (OC). These species are observed from various observational networks over southeastern US, such as the Clean Air Status and Trends Network (CASTNET), the Interagency Monitoring of Protected Visual Environments (IMPROVE), the Speciation Trends Network (STN), the Aerometric Information Retrieval System–Air Quality System (AIRS-AQS), and the Southeastern Aerosol Research and Characterization (SEARCH). The locations of these sites are plotted in Fig. 2. Column concentrations are evaluated over Southeastern US, including tropospheric carbon monoxide (CO) retrieved from the Measurements Of Pollution In The Troposphere (MOPITT, https://www2.acom.ucar.edu/mopitt), tropospheric nitrogen dioxide (NO_2) retrieved from the SCanning Imaging Absorption spectroMeter for Atmospheric CHartographY (SCIAMACHY, http://www.sciamachy.org/), and tropospheric O_3 residual (TOR) retrieved from the Aura Ozone Monitoring Instrument in combination with Aura Microwave Limb Sounder (OMI/MLS, http://acdb-ext.gsfc.nasa.gov/Data_services/cloud_slice/new_data.html). The protocols for performance evaluation include spatial distributions and statistics, following the ap-

GMDD
8, 9965–10009, 2015

proach of Zhang et al. (2006, 2009). The analysis of the performance statistics focus on mean bias (MB), normalized mean bias (NMB), normalized mean error (NME), root mean square error (RMSE), and correlation coefficient (Corr.). The definitions of those statistics can be found in Yu et al. (2006) and Zhang et al. (2006).

3 Simulation results and evaluation

3.1 Impacts of cumulus parameterizations

3.1.1 Meteorological predictions

Figure 3a and b shows the absolute differences in meteorology, cloud/radiative variables, and chemical predictions between SEN1 and BASE. Compared to BASE, SEN1 predicts higher T2 over most land area, and lower T2 over part of oceanic area. The increases of T2 in SEN1 can be up to 0.76 °C and the decrease of T2 can be up to 0.4 °C, with a domain averaged increase of 0.06 °C. The increase of T2 over land and decrease of T2 over ocean are mainly due an increase of SWD by 5.2 $W m^{-2}$ over land and a decrease of SWD by 2.5 $W m^{-2}$ over ocean. Q2 decreases in SEN1 over most of domain, with a domain averaged decrease of 0.3 $g kg^{-1}$, indicating much drier conditions predicted in SEN1. GF scheme is designed to be less active as the grid size reduces to cloud resolving scales. As a result, precipitation decreases in SEN1 over most of domain, with a domain averaged reduction of 3.6 mm day^{-1}. The reduction of the precipitation is mainly from the combined changes of increase in convective precipitation (by domain averaged of 2.7 mm day^{-1}) and decrease in non-convective precipitation (by domain averaged of 6.3 mm day^{-1}). Due to the more convection in SEN1, PBLH (Figure not shown) predicted by SEN1 also increases up to 185 m, with a domain averaged increase of 50.6 m.

Due to higher T2 and lower Q2 predicted by SEN1, less water vapor can condense onto the CCN surface. As a result, SEN1 predicts smaller cloud droplets than BASE.

GMDD
8, 9965–10009, 2015

CDNC predicted by SEN1 varies throughout the domain, with increases up to 993 cm^{-3} and decreases up to 749 cm^{-3}, resulting in a domain averaged increase of 3 cm^{-3} Small cloud droplets in SEN1 can deplete the available liquid water during their growth, which leads to reduction in LWP and CF. As a result, SEN1 predicts lower CF and LWP, with a domain averaged decrease of 6.6 % and 17.7 $g\,m^{-2}$, respectively. However, COT increases in SEN1, with a domain averaged increase of 16.0. The increase of COT is likely due to the decrease of cloud effective radius from smaller cloud droplets in SEN1. Although both CDNC and COT increase over land, the significant decrease of CF and LWP over land can result in a decrease in cloud albedo, and therefore a decrease in SWCF over land and near coastal areas in SEN1. The increase of SWCF over remote ocean is mainly due to the increase of CDNC and COT over these regions. As a result, compared to BASE, SEN1 predicts higher SWCF up to 49 $W\,m^{-2}$ and lower SWCF up to 45.3 $W\,m^{-2}$, with a domain averaged decrease of 1.7 $W\,m^{-2}$. The decrease or increase in SWCF can result in an increase or a decrease, respectively, in SWD. Compared to BASE, SEN1 predicts higher SWD by up to 52.71 $W\,m^{-2}$ and lower SWD by up to 51.8 $W\,m^{-2}$, with a domain averaged of 1.4 $W\,m^{-2}$.

Table 3a and Fig. 4 show the model performance of BASE and SEN1. Meteorological variables such as T2, RH2, and SST are well predicted in both BASE and SEN1, with NMBs within ± 6 %, and with slightly better performance in SEN1. WS10 is moderately underpredicted against observations at the NCDC sites in both BASE and SEN1, with NMBs of −58.3 and −61.3 %, respectively, whereas it is well predicted against the observations at the CASTNET sites, with NMBs of 5.4 and 4.9 %, respectively, for BASE and SEN1. With GF in SEN1, PBLH is impacted significantly over ocean, with increasing NMBs from 0.2 in BASE to 16.2 % in SEN1. Both LHFLX and SHFLX are overpredicted in BASE and SEN1, which is mainly due to lack of representations of the air–sea interactions. Compared to BASE, SEN1 improves the predictions of Precip over land (ocean) significantly, by reducing NMBs of 95.9 % (335.2 %) to 31.7 % (211.5 %) against GPCP and reducing NMBs of 111.5 % (42.2 %) to 218.8 % (128.2 %) against TMPA. CF is also improved by reducing NMBs from 23.7 in BASE to −1.0 % in

GMDD
8, 9965–10009, 2015

SEN1 over land, and from 48.7 % in BASE to 42.3 % in SEN1 over ocean, compared to CERES SYN1deg observations. LWP is more underpredicted with NMBs from −35.0 in BASE to −80.7 % in SEN1 over land but improved substantially over ocean with NMBs from 304.6 % in BASE to 35.1 % in SEN1. The significant decrease of LWP over ocean is likely due to higher CDNC associated with smaller cloud effective radius, resulting from less precipitation in SEN1. The performance of COT is improved over land with NMBs reducing from −70.3 in BASE to −39.5 % in SEN1 whereas it is degraded over ocean, with NMBs increasing from −21.8 % in BASE to 64.6 % in SEN1. The large overpredictions of COT over ocean are likely due to the smaller cloud effective radius in SEN1, which indicates the uncertainties in the treatments of cloud dynamics and thermodynamics. Compared to MODIS data, PWV over land is more underpredicted, with NMBs from −0.5 in BASE to −5.5 % in SEN1, and the performance of PWV over ocean is from overprediction by 3.2 % in BASE to underprediction by 4.2 % in SEN1. As shown in Fig. 4, the performance of AOD over land is slightly degraded with NMBs from −10.8 in BASE to −11.5 % in SEN1 and the performance of AOD over ocean is slightly improved with NMBs from −1.0 in BASE to −0.3 % in SEN1. The predictions of CCN5 are improved in SEN1, with NMBs from 21.1 in BASE to −0.8 % in SEN1. The decreases of CCN5 in SEN1 are mainly due to the lower aerosol number concentrations in SEN1. The overpredictions of CDNC are largely due to the uncertainties in the observations as there are only a few grid cells that contain observations.

Model predictions of radiative variables such as LWD, SWD, and OLR are comparable in BASE and SEN1, with slightly better performance of LWD over ocean (NMBs of 0.8 vs. 0.3 % for BASE and SEN1, respectively), SWD over land (NMBs of −2.4 vs. 0.5 %), and OLR over land (NMBs of −13.9 vs. −7.0 %) and ocean (NMBs of −22.9 vs. −20.7 %) in SEN1. On the other hand, there are significant changes in SWCF and LWCF. Compared to BASE, the domain averaged SWCF predicted by SEN1 decreases from −72.1 to −66.5 $W m^{-2}$ over land (with NMBs reduced from 57.2 to 45.1 %), and it increases from −118.1 to −120.2 $W m^{-2}$ over ocean (with NMBs increased slightly from 108.9 to 112.5 %). The domain averaged LWCF predicted by SEN1 decreases from

GMDD
8, 9965–10009, 2015

53.2 to 37.7 $W m^{-2}$ over land (with NMBs reduced significantly from 61.7 to 18.9 %), and it decreases from 77.8 to 74.5 $W m^{-2}$ over ocean (with NMBs reduced from 152.1 to 141.4 %). The improvements of SWCF and LWCF over land are attributed to the improvement of cloud variables (e.g., CF and COT) over land. The large overpredictions of SWCF and LWCF over ocean are attributed to the inaccurate predictions clouds over ocean, indicating the model uncertainties in the cloud dynamics and thermodynamics.

3.1.2 Chemical predictions

As shown in Fig. 3b, compared to BASE, SEN1 predicts higher surface CO and SO_2, with domain averaged of 5.6 and 0.05 ppb, respectively. The increased mixing ratios of CO and SO_2 are likely due to the lower chemical loss through oxidation by lower OH levels and less wet deposition resulted from lower precipitation in SEN1. The increase of surface mixing ratios of NO_2 over land is likely due to less wet deposition, and the decrease of surface mixing ratio of NO_2 over ocean is likely due to the increase of more convection over ocean (e.g., higher PBLH). The increase of surface O_3 mixing ratios over eastern land areas and east coast in SEN1 is likely due to the increase of NO_2 surface mixing ratios and the decrease of surface mixing ratios of O_3 over remote ocean is likely due to the more convection in SEN1. The decrease of surface mixing ratio of O_3 over southwestern areas of the domain is likely due to the more chemical loss through oxidation with alkenes (e.g., isoprene and terpene) under more stable and warmer conditions over these regions. Compared to BASE, SEN1 predicts higher SO_4^{2-} by up to 1.0 $\mu g m^{-3}$ and lower SO_4^{2-} by up to 1.6 $\mu g m^{-3}$. The increase of SO_4^{2-} over oceanic areas and some land areas is mainly due to the increase of surface mixing ratios of SO_2 and decrease of wet deposition. The decrease of SO_4^{2-} concentration over some land areas is mainly due to the decrease of chemical production from lower OH levels over these regions. The increase of SOA concentrations is mainly due to the increase of ASOA (by domain-average of 0.21 $\mu g m^{-3}$) and BSOA (by domain-average of 0.34 $\mu g m^{-3}$). Higher concentrations of ASOA can be attributed to less wet

GMDD
8, 9965–10009, 2015

deposition and higher gaseous precursors of SOA due to less wet deposition. Higher concentrations of BSOA can be attributed to less wet deposition and higher biogenic emissions resulted from higher SWD and T2 in SEN1. Compared to BASE, SEN1 predicts higher $PM_{2.5}$ and PM_{10} up to 4.9 $\mu g\,m^{-3}$, with a domain averaged increase of 0.68 and 0.17 $\mu g\,m^{-3}$, respectively. Unlike $PM_{2.5}$ concentrations that increase over most of the domain, the concentrations of PM_{10} decrease over remote ocean, which is mainly due to the decrease of sea-salt concentrations resulted from lower WS10 in SEN1.

Table 3b shows the statistical performance for chemical predictions. As precipitation is reduced in SEN1, the concentrations of gases and aerosols are less underpredicted or more overpredicted, with better performance for surface SO_2 (with NMBs changed from −43.7 % in BASE to −23.0 % in SEN1 against SEARCH), EC (with NMBs changed from −71.2 % in BASE to −63.1 % in SEN1 against SEARCH), OC (with NMBs changed from −44.1 % in BASE to −0.4 % in SEN1 against SEARCH), TC (with NMBs changed from −16.2 in BASE to 1.0 % in SEN1 against STN and from −40.3 % in BASE to 1.5 % in SEN1 against SEARCH), $PM_{2.5}$ (with NMBs changed from −22.2 in BASE to −12.0 % in SNE1 against IMPROVE, and from −29.3 % in BASE to −25.1 % in SEN1 against STN), PM_{10} (with NMBs changed from −65.4 in BASE to −62.1 % in SEN1 against AIRS-AQS), and column SO_2 (with NMBs changed from −68.8 % in BASE to −63.8 % in SEN1 against SCIAMACHY).

3.2 Impacts of atmosphere–ocean coupling

3.2.1 Impacts on meteorology

Figure 5a and b compares satellite observations/reanalysis data with model predictions by SEN1 (WRF/Chem without air–sea interactions), SEN2 (WRF/Chem-OML model), and SEN3 (WRF/Chem-ROMS). With the 1-D OML coupling, the predictions of most meteorological, cloud, and radiative variables are comparable in SEN1 and SEN2. For example, SST and PBLH slightly decrease by a domain averaged of 0.1 °C and 1.2 m, respectively, over ocean in SEN2 compared to SEN1. The 1-D OML model represents

GMDD
8, 9965–10009, 2015

the cooling of SST due to deep mixing of the ocean layers below with stably stratified cooler water. This cools the mixed layer, which reduces the SST and hence surface fluxes. In SEN2, LHFLX increases by 0.7 $W m^{-2}$ and SHFLX increases by 0.1 $W m^{-2}$ over ocean compared to SEN1. The negative correlation between LHFLX and SST indicates the dominance of atmospheric forcing of the ocean in western Atlantic Ocean and the contribution of atmospheric forcing to SST variations in these regions. However, due to the simplified assumptions and treatments in 1-D OML, the impacts of the 1-D ocean mixed layer on SWD and LHFLX are small, with domain averaged increases of SWD and LHFLX by 0.5 and 0.4 $W m^{-2}$, respectively.

With atmosphere–ocean coupling in WRF/Chem-ROMS used in SEN3, boundary layer properties predicted by WRF/Chem show some significant differences. For example, SEN3 predicts lower monthly-mean SST by up to 1.9 °C, with a domain averaged decrease of 0.9 °C. SST is prescribed in SEN1, whereas it is prognostic in WRF/Chem-ROMS in SEN3. The decrease of SST in SEN3 is mainly due to the lower SST from initial conditions from global HYCOM. SEN3 also predicts lower PBLH over ocean, with a domain averaged decrease of 56.5 m, indicating a more stable boundary condition in SEN3. The decrease of PBLH is mainly due to the decrease of heat fluxes through interactions with ocean. T2 and SST decrease in SEN3, resulting in less evaporation. As a result, SEN3 predicts lower LHFLX by up to 128.6 $W m^{-2}$, with a domain averaged decrease of 27.6 $W m^{-2}$. Comparing SEN3 to SEN1, the LHFLX-SST correlation is positive, suggesting the dominance of oceanic forcing of atmosphere in the western Atlantic Ocean. Due to the less evaporation in SEN3, precipitation and cloud are also reduced, resulting in higher SWD, with a domain averaged increase of 9.7 $W m^{-2}$.

As shown in Fig. 4, the prescribed SSTs in SEN1 agree relatively well with observations from OAFlux, with an NMB of 0.6 %. SST is relatively well predicted in SEN2, with an NMB of 0.4 %, whereas it is slightly underperdicted in SEN3, with NMBs of −2.8 %. SEN1 is forced simulations with prescribed SST from NCEP, whereas SST is prognostic in SEN2 and SEN3 with SST updated every model time step (i.e., 60 s) and every 10-min, respectively. However, the coupling with the 1-D OML causes very small

GMDD
8, 9965–10009, 2015

changes in the simulated SST, the resulted SST from SEN2 is quite similar to those based on the NCEP reanalysis data. Both SEN1 and SEN2 show warm SST bias for Gulf Stream (see Fig. 5a), whereas SEN3 gives cold bias for SST. The cold bias for SST in SEN3 can be attributed in part to the lower ICs and BCs from HYCOM-NCODA, and in part to the coarse vertical resolution in the ocean layers used in HYCOM (Hofmeister et al., 2010; Shapiro et al., 2013). A comparison of SST predictions from HYCOM with satellite retrievals indicates lower values from this model, especially near the coast, due likely to the inherent uncertainties in the model setting (e.g., the surface layer depth used for SST calculation is larger in the simulations at a coarse grid resolution than at a fine grid resolution).

In SEN1 and SEN2, warm SSTs can increase evaporation and convective instability. As a result, an atmospheric circulation that produces moisture convergence and convection occurs in response to SST gradients. Compared to NCEP/NARR reanalysis data, both SEN1 and SEN2 overpredict PBLH over ocean, with NMBs of 16.2, and 16.0 %, respectively, whereas SEN3 predicts PBLH well, with an NMB of −3.1 %. Compared to GPCP data, precipitation is largely overpredicted over ocean in both SEN1 and SEN2, with NMBs of 211.5 and 210.3 %, respectively, whereas it is significantly improved in SEN3, with an NMB of 119.2 %. Compared to TMPA data, precipitation is moderately overpredicted over ocean in SEN3, with an NMB of 60.6 %. The overpredictions of precipitation over ocean are likely due in part to the uncertainties in the convective precipitation and the satellite retrievals. LHFLX/SHFLX (see Table 3a) are largely overpredicted in SEN1 and SEN2, with NMBs of 60.1 %/138.2 %, and 60.7 %/140.7 %, respectively, whereas they are improved in SEN3 significantly, with NMBs of 18.9 %/50.2 %. SST simulated from SEN2 is very similar to SST based on the reanalysis data, which can drive atmospheric anomalies, and therefore generate larger monthly mean precipitation and LHFLX anomalies compared to the coupled simulation SEN3, especially over the regions with warm SST and high precipitation (e.g., Gulf Stream). In SEN3, with strong ocean advection simulated in the 3-D ROMS, warm ocean water moves from low latitude, resulting in warm SST in the Gulf Stream.

GMDD
8, 9965–10009, 2015

SST anomalies can induce opposite atmospheric changes in coupled atmosphere–ocean simulation SEN3 (Wu and Kirtman, 2005, 2007). As a result, the biases in the atmospheric predictions (e.g., WS10, PBLH, Precip, LHFLX, and SHFLX) are smaller in SEN3 than in SEN1 and SEN2.

Predictions of most cloud variables are comparable in SEN1 and SEN2 but are improved in SEN3, especially over ocean. Figure 5b compares satellite observations with predictions of AOD, CCN5, COT, and SWCF by SEN1, SEN2, and SEN3. Compared to SEN1, SEN3 predicts slightly higher AOD up to 0.038, and slightly lower AOD up to 0.048. The higher AOD can be attributed to the higher aerosol concentrations due to less wet deposition in SEN3. Compared to MODIS data, both SEN1 and SEN3 overpredict AOD over land by 1.5 and 3.5 %, respectively, and underpredict AOD over ocean by 34.6 and 31.5 %, respectively. The underpredictions of AOD over ocean are likely due to the inaccurate predictions of marine aerosols (e.g., sea-salt). Compared to SEN1, column concentration of CCN5 is lower in SEN3 over most domain, with a domain averaged decrease of $3.1 \times 10^{-7}\,\mathrm{cm}^{-2}$. Compared to MODIS data, column concentration of CCN5 over ocean is underpredicted by both SEN1 and SEN3, with NMBs of −0.8 and −12.7 %, respectively. The underpredictions of CCN5 are likely due to the inaccurate predictions of aerosol number concentrations, and uncertainties in the cloud thermodynamics. Compared to SEN1, SEN3 predicts higher COT up to 62.2, and lower COT up to 87.4, with a domain averaged decrease of 3.9. Compared to satellite data, both SEN1 and SEN3 underpredict COT over land, with NMBs of −39.5 and −39.8 %, respectively, and they overpredict COT over ocean, with NMBs of 64.6 % and 37.5 %, respectively. The biases in COT predictions are likely due to the model uncertainties in cloud dynamics and thermodynamics, as well as aerosol-cloud interactions. Compared to SEN1, SEN3 predicts higher SWCF up to $21.0\,\mathrm{W\,m}^{-2}$ over land, and lower SWCF up to $77.9\,\mathrm{W\,m}^{-2}$ over ocean, with a domain averaged decrease of $10.9\,\mathrm{W\,m}^{-2}$. The decrease of SWCF in SEN3 is mainly due to the decreases of COT and CDNC in SEN3. Compared to satellite data, the prediction of SWCF is improved over ocean significantly, with NMBs from 112.5 % in SEN1 to 78.5 % in SEN3. Other

GMDD
8, 9965–10009, 2015

cloud/radiative variables are also improved over ocean. For example, CF is improved over ocean, with NMBs from 42.3 % in SEN1 to 36.7 % in SEN3. LWP is improved over ocean, with NMBs from 35.1 % in SEN1 to −29.2 % in SEN3. Due to the improved cloud predictions, the performance of most radiative variables in SEN3 is also improved over ocean. For example, the prediction of SWD is improved over ocean with NMBs from −20.6 % in SEN1 to −13.7 % in SEN3. Predictions of OLR and LWCF are improved over ocean as well, with NMBs reduced from −20.7 in SEN1 to −16.8 % in SEN3, and from 141.4 in SEN1 to 107.7 % in SEN3, respectively.

3.2.2 Impacts on chemistry

Figure 6a and b shows the absolute differences between SEN2 and SEN1, and between SEN3 and SEN1 for surface chemical predictions. With 1-D OML model, the changes of most surface chemical species are small. For example, the differences in surface CO mixing ratios between SEN2 and SEN1 are within 11 ppb (or within 3 %). The absolute differences in surface mixing ratios of SO_2, NO_2, O_3, and OH are within 2 ppb, and the percentage differences can be as large as 29.8, 14.4, 6.5, and 9.8 %, respectively. Although the absolute differences in surface concentrations of SO_4^{2-}, SOA, $PM_{2.5}$, and PM_{10} are within 1.5 $\mu g\,m^{-3}$, the percentage differences can be as large as 20.2, 757.5, 9.0, and 11.7 %, respectively. The significant change of SOA concentrations up to 0.4 $\mu g\,m^{-3}$ in SEN2 is likely due to higher OH levels and lower PBLH over southeastern domain (e.g., 31–34° N). With coupling of 3-D ROMS, the changes in the concentrations of most surface chemical species between SEN3 and SEN1 are much larger than those between SEN2 and SEN1. For example, surface CO mixing ratios can increase as large as 196.5 ppb and decrease as large as 304.9 ppb. Although the absolute differences in the surface mixing ratios of SO_2 and OH between SEN1 and SEN3 are within 1.5 ppb, the percentage differences in the surface mixing ratios of SO_2 and OH can be as large as 134.4 and 83.6 %, respectively. The changes of the surface mixing ratios of NO_2 and O_3 are also significant, which can be as large as 18.0 ppb

GMDD
8, 9965–10009, 2015

(or 189.2 %) and 17.3 ppb (or 44.8 %), respectively. The decreases of the mixing ratios of CO, SO_2, and NO_2 are likely due in part to the enhanced oxidation with higher OH concentrations in SEN3. The increase in OH concentrations can be attributed to the decrease of precipitation and PBLH, and the increase of SWD in SEN3. Compared to SEN1, surface SO_4^{2-} concentrations predicted by SEN3 can increase as large as 0.9 $\mu g\,m^{-3}$ and decrease as large as 1.2 $\mu g\,m^{-3}$. The changes in surface SO_4^{2-} predictions are mainly due in part to changes in the mixing ratios of SO_2 and OH through gas-phase oxidation, changes in cloud fraction through aqueous-phase chemistry, and changes in precipitation. Surface SOA predicted by SEN3 can increase as large as 0.7 $\mu g\,m^{-3}$ and decrease as large as 1.5 $\mu g\,m^{-3}$. The changes in SOA predictions are likely due to the combined changes in OH mixing ratios, precipitation, SWD, and PBLH. There are similar patterns in changes of surface concentrations of $PM_{2.5}$ and PM_{10} over land. Both $PM_{2.5}$ and PM_{10} increase over 30–33° N, and decrease over 33–40° N. The increase of $PM_{2.5}$ can be as large as 3.0 $\mu g\,m^{-3}$ and the decrease of $PM_{2.5}$ can be as large as 7.9 $\mu g\,m^{-3}$. The changes of $PM_{2.5}$ over land are mainly due to the changes in SO_4^{2-}, NH_4^+, and SOA, which can be attributed to the changes in precipitation and PBLH over land, and the changes of $PM_{2.5}$ over ocean are mainly due to the changes in SO_4^{2-}, NH_4^+, NO_3^-, SOA, and sea-salt, which can be attributed to the combined effects of changes in precipitation, PBLH, and WS10. The decreases of PM_{10} over remote ocean are mainly due the decreases in sea-salt predictions resulted from lower WS10 in SEN3 than SEN1. As shown in Fig. 6b, most significant changes in surface chemical predictions are along coast, over remote ocean, and part of inland regions, indicating the significant impacts of air–sea interactions on air quality. The changes in surface chemical predictions over inland regions are mainly caused by the changes in meteorology (e.g., T2, PBLH, WS10, SWD, and Precip) over these regions resulted from coupling of ROMS with WRF/Chem.

Figure 7a and b shows the time series observations and model predictions over coastal sites from CASTNET, IMPROVE, and AIRS-AQS for surface max 8 h mixing ratios of O_3 and $PM_{2.5}$. Compared to SEN1, the differences in Max 8 h O_3 can be as large

GMDD
8, 9965–10009, 2015

as about 15 ppb at the CASTNET sites. Max 8 h O_3 mixing ratios predicted by SEN1, SEN2, and SEN3 overall correlate well with observations at the CASTNET sites, with a better performance by SEN3 over BFT142 and IRL141. Compared to SEN1, the differences in Max 8 h O_3 mixing ratios can be as large as about 20 ppb over the AQS sites. Max 8 h O_3 mixing ratios from SEN3 are large overpredicted by three simulations at the AQS sites such as site Holiday, FL (121 012 001) and site Gulfport Youth Court, MS (280 470 008). As shown in Fig. 7b, $PM_{2.5}$ is overall well predicted at the IMPROVE and AQS sites. Compared to SEN1, the differences in surface $PM_{2.5}$ predictions from SEN3 can be as large as about 15 $\mu g\,m^{-3}$ at the IMPROVE sites and as large as about 6 $\mu g\,m^{-3}$ at the AQS sites, with a better performance by SEN3 at the four sites: CHAS1, ROMA1, EVER1, and SWAN1. Due to the relatively coarse grid resolution used in this work, The model shows some difficulties in capturing the observed temporal variations of O_3 during some time periods at some sites (e.g., overpredictions at Holiday, FL during most days, and at Gulfport Youth Court after 15 July). Figure 8 shows the scatter plots for major chemical species over various observational networks. Compared to SEN1, SEN3 predicts overall better chemical concentrations. For example, surface predictions of gaseous species such as SO_2 and HNO_3 are improved by reducing NMBs from 204.5 to 192.1 %, and from 92.4 to 85.1 %, respectively. Hourly O_3 prediction is also slightly improved by reducing NMBs from 27.3 to 26.4 % against the AIRS-AQS sites. Predictions of max 1 h and 8 h O_3 mixing ratios are also improved by reducing NMBs from 3.0 to 2.1 % against CASTNET (15.6 to 14.8 % against AIRS-AQS), and 13.2 to 12.2 % against CASTNET (20.0 to 19.2 % against AIRS-AQS), respectively. Model predictions of aerosol species such as SO_4^{2-}, NH_4^+, and NO_3^- are slightly or moderately improved against STN observations. The concentrations of Na^+ and Cl^- are largely underpredicted in both SEN1 and SEN3, indicating the uncertainties in the online sea-salt emission modules. In SEN3, the model performance of EC is slightly improved at the IMPROVE sites but slightly degraded at the SEARCH sites, whereas the model performance of OC and TC is slightly degraded at the IMPROVE sites but slightly improved at the SEARCH sites. $PM_{2.5}$ prediction is slightly improved in SEN3

GMDD
8, 9965–10009, 2015

at the IMPROVE sites, but degraded at the STN sites. PM_{10} prediction is also slightly improved in SEN3, with NMBs reduced from −62.1 to −61.7 %. The large underpredictions of PM_{10} are likely due to the inaccurate predictions of sea-salt concentrations and the overpredictions of precipitation over land. The predicted column concentrations of NO_2, CO, and TOR are comparable in SEN1 and SEN3, with slightly better performance of column SO_2.

4 Conclusions

In this work, different cumulus parameterization schemes are tested in WRF/Chem to study the sensitivity of cumulus schemes on model predictions. In addition, 1-D OML and 3-D ocean coupling with WRF/Chem are used to study the impacts of air–sea interactions on air quality predictions. Due to the consideration of resolving subgrid-scale clouds, SEN1 with GF scheme can predict much better precipitation compared to BASE with G3D scheme, with NMBs reduced from 95.9 to 35.7 % over land, and from 335.2 to 211.5 % over ocean against GPCP. Compared to BASE, SEN1 improves model performance for most cloud and radiative variables, such as CF, COT, LWD, SWD, and OLR, mainly over ocean. Due to the improvement in cloud predictions, SWCF and LWCF predictions are also improved. However, the large overpredictions of clouds and radiative forcing over ocean indicate the model uncertainties in the cloud dynamics and thermodynamics, as well as aerosol-cloud interactions. The changes in meteorology, clouds, and radiation in SEN1 can impact chemical predictions. As precipitation is reduced in SEN1, gases and aerosols are less underpredicted or more overpredicted, with better performance of surface predictions of TC, $PM_{2.5}$, PM_{10}, and column SO_2 in SEN1 than BASE.

With the inclusion of ocean coupling in SEN2 and SEN3, simulated boundary layer properties are changed. As OML is a simplified 1-D model with large uncertainty, the impacts on boundary layer are not as significant as those of the coupling of WRF/Chem with the 3-D ROMS, which consists of detailed primitive equations for 3-D ocean circu-

GMDD
8, 9965–10009, 2015

lation and dynamics. Although SEN2 predicts SST, the coupling with the 1-D OML results in small changes in SST from the initial SST that is based on the NCEP reanalysis data. The warm bias of SST from SEN2 over Gulf Stream can generate larger monthly mean rainfall and surface latent heat flux anomalies compared to SEN3, whose SST is prognostic in ROMS and it is changed more obviously than that in SEN2. As a result, the model predictions of precipitation, LHFXL, and SHFLX are improved significantly in SEN3, with NMBs significantly reduced from 211.5 % in SEN1 to 119.2 % in SEN3, from 60.1 % in SEN1 to 18.9 % in SEN3, and from 138.2 % in SEN1 to 50.2 % in SEN3, respectively. However, compared to the observations of OAflux, SST in SEN3 is slightly underpredicted with an NMB of −2.8 %, which is mainly due to the lower initial conditions from global HYCOM data. Due to the improvement in the predictions of surface heat fluxes, PBLH predictions are also improved in SEN3, with NMBs reduced from 16.2 % in SEN1 to −3.1 % in SEN3 over ocean. Due to more stable boundary layer and less evaporation over ocean in SEN3, the predictions of most cloud variables such as CF, COT, and LWP over ocean are also improved in SEN3. As a result, the predictions of radiative variables such as SWD, OLR, SWCF, and LWCF over ocean are also improved.

Due to the changes in the boundary layer properties, surface chemical predictions are affected significantly in SEN3. For example, With the coupling of WRF/Chem with 1-D OML model, surface levels of O_3 and $PM_{2.5}$ can increase as large as 1.8 ppb and 1.0 $\mu g\,m^{-3}$, and decreases as large as 1.4 ppb and 1.1 $\mu g\,m^{-3}$, with a domain averaged increase of 0.03 ppb and 0.02 $\mu g\,m^{-3}$, respectively. With the coupling of WRF/Chem with the 3-D ROMS, surface O_3 and $PM_{2.5}$ concentrations can increase as large as 12.0 ppb and 3.0 $\mu g\,m^{-3}$, and decreases as large as 17.3 ppb and 7.9 $\mu g\,m^{-3}$, with a domain averaged decrease of 0.67 ppb and 0.08 $\mu g\,m^{-3}$, respectively. The largest differences in surface O_3 predictions are along the coastal areas and remote ocean, whereas the largest differences in surface $PM_{2.5}$ predictions are not only along the coastal areas and remote ocean, but also over inland areas, indicating the significant impacts of air–sea interactions on chemical predictions. Compared to SEN1, SEN3

GMDD
8, 9965–10009, 2015

shows overall better performance for chemical concentrations of SO_2, HNO_3, Max 1 h and 8 h O_3, SO_4^{2-}, NH_4^+, and NO_3^-, and PM_{10}. The simulated column concentrations are comparable in SEN1 and SEN3, with slightly better performance of column SO_2 in SEN3.

There are several limitations in this work. First, cold biases exist in the SST simulated by WRF/Chem-ROMS. Using an alternative ICs and BCs for ROMS based on other ocean models, such as the Global Ocean Physical Reanalysis System (GLORS) (http://www.cmcc.it/it/models/c-glors-the-cmcc-global-ocean-physical-reanalysis-system) and the Simple Ocean Data Assimilation (SODA) (http://www.atmos.umd.edu/~ocean/data.html) may reduce such cold biases in SST, which will in turn improve meteorological and chemical predictions of WRF/Chem-ROM. Second, large biases remain in the predictions of some meteorological (e.g., WS10 over land and precipitation over ocean) and cloud variables (e.g., COT, CDNC, LWP, and SWCF), indicating the model uncertainties in the model representations of boundary layer, convection, cloud dynamics and thermodynamics, as well as aerosol-cloud interactions. Those are the research areas that may lead to improved model performance for future work. Finally, when computational resources become available, finer grid resolution (e.g., 1–4 km) may be applied in the future to better capture the fine-scale features along the coast.

Code and data availability

WRF/Chem with the CB05-MADE/VBS option used in this work has been incorporated into the WRF/Chem version 3.7, which is available for download at http://www.mmm.ucar.edu/wrf/users/. The COAWST model is based on version 3.1 (as of August 2014), which available for download at https://coawstmodel.sourcerepo.com/coawstmodel/COAWST.

Upon request, we will provide the inputs including the meteorological files, meteorological and chemical initial and boundary conditions, model the namelist set-up, and a brief instructions on for a 1 day test case. We can also provide sample outputs for the 1 day test.

GMDD
8, 9965–10009, 2015

Acknowledgement. This work is sponsored by the U.S. National Science Foundation EaSM program (Grant # AGS-1 049 200). R. He also thanks support provided by the USGS through Coastal Ocean Process Project (Grant # G14AC00044). MODIS data and CERES data are provided by NASA via http://ladsweb.nascom.nasa.gov/data/search.html and http://ceres.larc.nasa.gov/order_data.php, respectively. We would like to acknowledge high-performance computing support from Yellowstone (ark:/85065/d7wd3xhc) provided by NCAR's Computational and Information Systems Laboratory, sponsored by the U.S. National Science Foundation.

References

Ahmadov, R., McKeen, S. A., Robinson, A. L., Bahreini, R., Middlebrook, A. M., de Gouw, J. A., Meagher, J., Hsie, E.-Y., Edgerton, E., Shaw, S., and Trainer, M.: A volatility basis set model for summertime secondary organic aerosols over the eastern United States in 2006, J. Geophys. Res., 117, D06301, doi:10.1029/2011JD016831, 2012.

Binkowski, F. S. and Roselle, S. J.: Models-3 Community multiscale air quality (CMAQ) model aerosol component, 1 Model description, J. Geophys. Res., 108, 4183, doi:10.1029/2001JD001409, 2003.

Bennartz, R.: Global assessment of marine boundary layer cloud droplet number concentration from satellite, J. Geophys. Res., 112, D02201, doi:10.1029/2006JD007547, 2007.

Byun, D. W. and Schere, K. L.: Review of the governing equations, computational algorithms, and other components of the Models-3 Community Multiscale Air Quality (CMAQ) Modeling System, Appl. Mech. Rev., 59, 51–77, 2006.

ENVIRON: User's Guide to the Comprehensive Air Quality Model with Extensions (CAMx) Version 2.0, available at: http://www.camx.com (last access: June 2015), 1998.

ENVIRON: User's guide to the Comprehensive Air Quality Model with Extensions (CAMx). Version 5.2, available at: http://www.camx.com (last access: June 2015), 2010.

Fast, J. D., Gustafson Jr., W. I., Easter, R. C., Zaveri, R. A., Barnard, J. C., Chapman, E. G., and Grell, G. A.: Evolution of ozone, particulates, and aerosol direct forcing in an urban area using a new fully-coupled meteorology, chemistry, and aerosol model, J. Geophys. Res., 111, D21305, doi:10.1029/2005JD006721, 2006.

GMDD

8, 9965–10009, 2015

Grell, G. A. and Freitas, S. R.: A scale and aerosol aware stochastic convective parameterization for weather and air quality modeling, Atmos. Chem. Phys., 14, 5233–5250, doi:10.5194/acp-14-5233-2014, 2014.

Grell, G. A., Peckham, S. E., Schmitz, R., McKeen, S. A., Frost, G., Skamarock, W. C., and Eder, B.: Fully coupled "online" chemistry within the WRF model, Atmos. Environ., 39, 6957–6975, doi:10.1016/j.atmosenv.2005.04.027, 2005.

He, J., Zhang, Y., Glotfelty, T., He, R., Bennartz, R., Rausch, J., and Sartelet, K.: Decadal Simulation and Comprehensive Evaluation of CESM/CAM5.1 with Advanced Chemistry, Aerosol Microphysics, and Aerosol-Cloud Interactions, J. Adv. Model Earth Syt., 07, doi:10.1002/2014MS000360, 2015.

He, R. and Wilkin, J. L.: Barotropic tides on the southeast New England shelf: a view from a hybrid data assimilative modeling approach, J. Geophys. Res., 111, C08002, doi:10.1029/2005JC003254, 2006.

He, R., McGillicuddy Jr., D. J., Keafer, B. A., and Anderson, D. M.: Historic 2005 toxic bloom of Alexandrium fundyense in the western Gulf of Maine: 2. Coupled biological numerical modeling, J. Geophys. Res., 113, C07040, doi:10.1029/2007JC004602, 2008.

Hofmeister, R., Burchard, H., and Beckers, J.-M.: Non-uniform adaptive vertical grids for 3D numerical ocean models, Ocean Model., 33, 70–86, doi:10.1016/j.ocemod.2009.12.003, 2010.

Marchesiello, P., McWilliams, J. C., and Shchepetkin, A.: Equilibrium structure and dynamics of the California current system, J. Phys. Oceanogr., 33, 753–783, 2003.

Nelson, J. and He, R.: Effect of the Gulf Stream on winter extratropical cyclone outbreaks, Atmos. Sci. Let., 13, 311–316, doi:10.1002/asl.400, 2012.

Nelson, J., He, R., Warner, J. C., and Bane, J.: Air–sea interactions during strong winter extratropicalstorms, Ocean Dynam., 64, 1233–1246, doi:10.1007/s10236-014-0745-2, 2014.

Pollard, R. T., Rhines, P. B., and Thompson, R. O. R. Y.: The deepening of the wind mixed layer, Geophys. Fluid Dyn., 3, 381–404, 1973.

Sarwar, G., Luecken, D., Yarwood, G., Whitten, G. Z., and Carter, W. P. L.: Impact of an updated carbon bond mechanism on predictions from the CMAQ modeling system: preliminary assessment, J. Appl. Meteorol. Clim., 47, 3–14, 2008.

Sarwar, G., Fahey, K., Napelenok, S., Roselle, S., and Mathur, R.: Examining the impact of CMAQ model updates on aerosol sulfate predictions, The 10th Annual CMAS Models-3 User's Conference, Chapel Hill, NC, October 2011.

GMDD
8, 9965–10009, 2015

Shapiro, G., Luneva, M., Pickering, J., and Storkey, D.: The effect of various vertical discretization schemes and horizontal diffusion parameterization on the performance of a 3-D ocean model: the Black Sea case study, Ocean Sci., 9, 377–390, doi:10.5194/os-9-377-2013, 2013.

Shchepetkin, A. F. and McWilliams, J. C.: The Regional Ocean Modeling System: a split-explicit, free-surface, topography following coordinates ocean model, Ocean Model., 9, 347–404, 2005.

Wang, K., Yahya, K., Zhang, Y., Wu, S.-Y., and Grell, G.: Implementation and initial application of a new chemistry-aerosol option in WRF/Chem for simulation of secondary organic aerosols and aerosol indirect effects, Atmos. Environ., 115, 716–732, 2014a.

Wang, K., Yahya, K., Zhang, Y., Christian, H., George, P., Christoph, K., Alma, H., Roberto, S. J., Juan, L. P., Pedro, J.-G., Rocio, B., Paul, M., and Ralf, B.: A multi-model assessment for the 2006 and 2010 simulations under the Air Quality Model Evaluation International Initiative (AQMEII) phase 2 over North America: part I I. Evaluation of column variable predictions using satellite data, Atmos. Environ., 115, 587–603, doi:10.1016/j.atmosenv.2014.07.044, 2014b.

Warner, J. C., Armstrong, B., He, R., and Zambon, J. B.: Development of a coupled ocean–atmosphere-wave-sediment transport (COWAST) modeling system, Ocean Model., 35, 230–244, doi:10.1016/j.ocemod.2010.07.010, 2010.

Wu, R. and Kirtman, B. P.: Roles of Indian and Pacific Ocean air–sea coupling in tropical atmospheric variability, Clim. Dynam., 25, 155–170, 2005.

Wu, R. and Kirtman, B. P.: Regimes of seasonal air–sea interaction and implications for performance of forced simulations, Clim. Dynam., 29, 393–410, 2007.

Yahya, K., Wang, K., Gudoshava, M., Glotfelty, T., and Zhang, Y.: Application of WRF/Chem over the Continental U. S. Under the AQMEII Phase II: Comprehensive Evaluation of 2006 Simulation, Atmos. Environ., 115, 733–755, 2014.

Yahya, K., Wang, K., Zhang, Y., and Kleindienst, T. E.: Application of WRF/Chem over North America under the AQMEII Phase 2 – Part 2: Evaluation of 2010 application and responses of air quality and meteorology–chemistry interactions to changes in emissions and meteorology from 2006 to 2010, Geosci. Model Dev., 8, 2095–2117, doi:10.5194/gmd-8-2095-2015, 2015.

Yu, S.-C., Eder, B., Dennis, R., Chu, S.-H., and Schwartz, S: New unbiased symmetric metrics for evaluation of air quality models, Atmos. Sci. Lett., 7, 26–34, 2006.

GMDD
8, 9965–10009, 2015

Zhang, Y., P. Liu, B. Pun, and Seigneur, C.: A Comprehensive Performance Evaluation of MM5-CMAQ for the Summer 1999 Southern Oxidants Study Episode, Part- I. Evaluation Protocols, Databases and Meteorological Predictions, Atmos. Environ., 40, 4825–4838, 2006.

Zhang, Y., Vijayaraghavan, K., Wen, X.-Y., Snell, H. E., and Jacobson, M. Z.: Probing into regional ozone and particulate matter pollution in the United States: 1. A 1 year CMAQ simulation and evaluation using surface and satellite data, J. Geophys. Res., 114, D22304, doi:10.1029/2009JD011898, 2009.

Zhang, Y., Pan, Y., Wang, K., Fast, J. D., and Grell, G. A.: WRF/Chem-MADRID: incorporation of an aerosol module into WRF/Chem and its initial application to the TexAQS2000 episode, J. Geophys. Res., 115, D18202, doi:10.1029/2009JD013443, 2010.

Zambon, J. B., He, R., and Warner, J. C.: Investigation of Hurricane Ivan using the Coupled Ocean–Atmosphere–Wave–Sediment Transport (COAWST) Model, Ocean Dynam., 64, 1535–1554, doi:10.1007/s10236-014-0777-7, 2014a.

Zambon, J. B., He, R., and Warner, J. C.: Tropical to extratropical: marine environmental changes associated with Superstorm Sandy prior to its landfall, Geophys. Res. Lett., 41, 8935–8943, doi:10.1002/2014GL061357, 2014b.

GMDD
8, 9965–10009, 2015

Table 1. Simulation Design

Run Index	Description	Purpose
BASE	Baseline, NCSU's version of WRF/Chem v3.6.1 with the G3 cumulus parameterization	Severed as baseline
SEN1	Same as BASE, but with the GF cumulus parameterization	The differences between SEN1 and BASE indicate the impacts of different cumulus parameterizations on model predictions; Severed as the baseline to investigate the impacts of atmosphere–ocean coupling using 1-D OML and 3-D ROMS.
SEN2	Same as SEN1, but with WRF/Chem with the 1-D ocean mixed layer model (WRF/Chem-OML)	The differences between SEN2 and SEN1 indicate the impacts of 1-D ocean mixed layer model on model predictions
SEN3	Same as SEN1, but with WRF/Chem coupled with ROMS within the COAWST frame work (WRF/Chem-ROMS)	The differences between SEN3 and SEN1 indicate the impacts of the atmosphere–ocean coupling on model predictions

GMDD
8, 9965–10009, 2015

Table 2. Datasets for Model Evaluation

Species/Variables	Dataset	Spatial (Temporal) Resolution
Temperature at 2 m (T2), Relative humidity at 2 m (RH2), Wind speed at 10 m (WS10)	Land: NCDC, SEARCH; Ocean: NDBC	400 sites (hourly), 7 sites (hourly); 15 sites (hourly)
Planetary boundary layer height (PBLH)	NCEP/NARR	32 km (monthly)
Sea surface temperate (SST), sensible heat flux (SHFLX), latent heat flux (LHFLX)	OAFlux	1° (monthly)
Precipitation (Precip)	GPCP, TMAP	2.5° (monthly), 0.25° (daily)
Outgoing longwave radiation (OLR), Downwelling longwave radiation (LWD), Downwelling shortwave radiation (SWD), Shortwave cloud radiative forcing (SWCF), Longwave cloud radiative forcing (LWCF)	CERES-EBAF	1° (monthly)
Cloud fraction (CF), Cloud optical thickness (COT), Cloud liquid water path (LWP)	CERES-SYN1deg	1° (monthly)
Precipitating water vapor (PWV), Aerosol optical depth (AOD), Column cloud condensation nuclei (ocean) at $S = 0.5\,\%$ (CCN5),	MODIS	1° (monthly)
Cloud droplet number concentration (CDNC)	Bennartz (2007)	1° (monthly)
Max 1 h Ozone (O_3), Max 8 h O_3	CASTNET, AIRS-AQS	38 sites (hourly), 420 (hourly)

GMDD
8, 9965–10009, 2015

Table 2. Continued.

Species/Variables	Dataset	Spatial (Temporal) Resolution
Hourly O_3	AIRS-AQS, SEARCH	420 (hourly), 7 sites (hourly)
Sulfur dioxide (SO_2), Nitric acid (HNO_3)	CASTNET	38 sites (weekly)
Carbon monoxide (CO), Nitrogen dioxide (NO_2)	SEARCH	7 sites (hourly)
Sulfate (SO_4^{2-}), Ammonium (NH_4^+), Nitrate (NO_3^-)	CASTNET, IMPROVE, STN	38 sites (weekly), 29 sites (3 day), 74 sites (3 day to weekly)
Organic carbon (OC)	IMPROVE, SEARCH	29 sites (3 day), 7 sites (daily)
Elementary carbon (EC), Total carbon (TC)	IMPROVE, STN, SEARCH	29 sites (3 day), 74 sites (3 day to weekly) 7 sites (daily)
Particulate matter with diameter less than and equal to 2.5 µm ($PM_{2.5}$)	IMPROVE, STN, SEARCH	29 sites (3 day), 74 sites (3 day to weekly), 7 sites (daily)
Particulate matter with diameter less than and equal to 10 µm (PM_{10})	AIRS-AQS	53 sites (hourly)
Tropospheric CO	MOPITT	1° (monthly)
Tropospheric SO_2, NO_2	SCIAMCHY	0.25° (monthly)
Tropospheric ozone residual (TOR)	OMI/MLS	1.25° (monthly)

NCDC: National Climatic Data Center; NDBC: National Data Buoy Center; NCEP/NAAR: National Centers for Environmental Prediction and North American Regional Reanalysis; OAFlux: Objectively Analyzed Air–Sea Fluxes; GPCP: the Global Precipitation Climatology Project; TMAP: Multi-satellite Precipitation Analysis from the Tropical Rainfall Measuring Mission; CERES-EBAF: Clouds and Earth's Radiant Energy System Energy Balanced And Filled data product; CERES-SYN1deg: CERES Synoptic product at 1° spatial resolution; MODIS: Moderate Resolution Imaging Spectroradiometer; OMI/MLS: the Aura Ozone Monitoring Instrument in combination with Aura Microwave Limb Sounder; MOPITT: the Measurements Of Pollution In The Troposphere; the Global Ozone Monitoring Experiment; SCIAMCHY: the SCanning Imaging Absorption spectroMeter for Atmospheric CHartographY; CASTNET: Clean Air Status and Trends Network; IMPROVE: Interagency Monitoring of Protected Visual Environments; STN: Speciation Trends Network; SEARCH: Southeastern Aerosol Research and Characterization; AIRS-AQS: the Aerometric Information Retrieval System–Air Quality System.

GMDD
8, 9965–10009, 2015

Table 3. (a) Statistical Performance of Meteorological, Cloud, and Radiative Variables. **(b)** Statistical Performance of Chemical Species.

(a) Species/ Variables	Datasets	obs	BASE				SEN1				SEN2				SEN3			
			sim	NMB (%)	NME (%)	Corr	sim	NMB (%)	NME (%)	Corr	sim	NMB (%)	NME (%)	Corr	sim	NMB (%)	NME (%)	Corr
T2 (°C)	NCDC	26.6	25.3	−4.9	8.8	0.82	25.4	−4.3	8.4	0.83	25.4	−4.3	8.4	0.83	25.4	−4.4	8.4	0.83
	NDBC	27.8	27.3	−1.8	3.6	0.87	27.4	−1.4	3.4	0.89	27.4	−1.4	3.5	0.89	26.7	−3.7	6.0	0.74
	SEARCH	27.7	26.1	−5.8	8.4	0.74	26.2	−5.3	8.4	0.78	26.3	−5.1	7.6	0.78	26.2	−5.4	7.8	0.78
RH2 (%)	NCDC	73.9	74.6	1.0	14.8	0.67	73.6	−0.4	14.3	0.69	73.6	−0.4	14.3	0.68	73.7	−0.2	14.3	0.69
	SEARCH	75.5	78.8	4.4	13.7	0.64	77.3	2.4	12.7	0.70	77.3	2.4	12.6	0.70	77.7	2.9	12.9	0.69
WS10 ($m\ s^{-1}$)[1]	NCDC	6.8	2.8	−58.3	62.3	0.16	2.6	−61.3	63.6	0.20	2.6	−61.5	63.7	0.20	2.7	−60.6	63.1	0.21
	NDBC	5.5	6.9	25.1	48.2	0.28	6.1	10.6	34.4	0.47	6.1	10.1	34.5	0.47	5.9	7.1	30.6	0.56
	SEARCH	2.5	2.9	16.7	52.1	0.09	2.2	−12.6	34.4	0.17	2.2	−13.4	34.8	0.18	2.2	−14.2	34.3	0.20
Precip (mm day^{-1})	GPCP (land)	4.1	8.1	95.9	110.0	0.14	5.4	31.7	46.1	0.36	5.4	31.9	44.9	0.38	5.3	29.5	40.6	0.35
	GPCP (ocean)	3.9	16.8	335.2	339.7	0.18	12.0	211.5	215.5	0.24	12.0	210.3	214.7	0.25	8.5	119.2	124.5	0.37
	TMPA (land)	3.8	8.1	111.5	127.6	0.15	5.4	42.2	58.8	0.27	5.4	42.4	57.6	0.28	5.3	39.8	53.2	0.23
	TMPA (ocean)	5.3	16.8	218.8	223.8	0.30	12.0	128.2	133.4	0.38	12.0	127.3	132.4	0.40	8.5	60.6	73.4	0.46
SWD ($W\ m^{-2}$)[3]	CERES (land)	263.7	257.3	−2.4	8.8	0.36	262.5	−0.5	8.5	0.40	261.6	−0.8	8.4	0.35	261.2	−0.9	7.7	0.35
	CERES (ocean)	266.1	213.9	−19.6	19.8	0.51	211.4	−20.6	21.2	0.48	211.3	−20.6	21.3	0.48	229.6	−13.7	14.2	0.49
	CASTNET	272.4	295.3	8.4	34.7	0.88	299.7	10.0	34.6	0.88	298.8	9.7	35.1	0.88	299.3	9.9	34.3	0.88
	SEARCH	303.6	243.0	−20.0	43.7	0.76	256.5	−15.5	41.5	0.78	257.2	−15.3	40.6	0.80	251.9	−17.0	41.5	0.79
OLR ($W\ m^{-2}$)	CERES (land)	259.9	223.8	−13.9	14.0	0.48	241.7	−7.0	7.2	0.64	240.8	−7.3	7.5	0.64	241.7	−7.0	7.1	0.61
	CERES (ocean)	253.7	195.6	−22.9	22.9	0.33	201.1	−20.7	20.7	0.51	200.7	−20.9	20.9	0.51	211.1	−16.8	16.8	0.56
SWCF ($W\ m^{-2}$)	CERES (land)	−45.9	−72.1	57.2	61.8	0.32	−66.5	45.1	50.8	0.42	−66.5	45.1	50.9	0.39	−66.5	45.0	49.4	0.33
	CERES (ocean)	−56.6	−118.1	108.9	109.3	0.50	−120.2	112.5	113.7	0.47	−119.4	111.2	112.4	0.46	−100.9	78.5	79.3	0.54
CF (%)	CERES (land)	46.3	57.3	23.7	32.8	0.26	45.8	−1.0	27.1	0.32	45.7	−1.2	27.4	0.29	45.9	−0.9	26.7	0.29
	CERES (ocean)	53.3	79.8	48.7	50.2	0.16	75.9	42.3	46.1	0.14	75.9	42.3	46.2	0.14	72.9	36.7	39.3	0.20

GMDD
8, 9965–10009, 2015

Table 3. Continued.

(a) Species/ Variables	Datasets	obs	BASE				SEN1				SEN2				SEN3			
			sim	NMB (%)	NME (%)	Corr	sim	NMB (%)	NME (%)	Corr	sim	NMB (%)	NME (%)	Corr	sim	NMB (%)	NME (%)	Corr
COT	CERES (land)	34.8	10.3	−70.3	70.4	−0.38	21.1	−39.5	53.0	−0.39	21.0	−39.8	52.2	−0.44	21.0	−39.8	49.9	−0.35
	CERES (ocean)	26.2	20.5	−21.8	35.0	0.36	43.2	64.6	77.5	0.28	42.6	62.5	75.4	0.28	36.0	37.5	58.3	0.27
LWP ($g m^{-2}$)	CERES (land)	119.5	76.3	−35.0	87.2	−0.41	22.7	−80.7	87.0	−0.25	21.0	−82.2	87.6	−0.24	16.1	−86.3	88.1	−0.02
	CERES (ocean)	81.8	331.0	304.6	323.4	0.07	110.5	35.1	110.8	0.01	112.6	37.6	112.0	−0.00	57.9	−29.2	83.7	0.14
AOD	MODIS (land)	0.15	0.16	2.4	23.6	0.47	0.16	1.5	22.4	0.53	0.16	1.5	22.9	0.51	0.16	3.5	22.7	0.54
	MODIS (ocean)	0.21	0.14	−35.0	35.0	0.44	0.14	−34.6	34.9	0.34	0.14	−34.5	34.6	0.35	0.14	−31.5	32.2	0.29
CCN5 ($10^8 cm^{-2}$)	MODIS (ocean)	2.8	3.4	21.1	45.8	0.25	2.8	−0.8	42.5	−0.03	2.8	−0.7	42.7	−0.01	2.5	−12.7	40.3	0.07
CDNC	Bennartz (2007)	49.6	172.2	247.0	269.4	−0.04	132.7	167.4	256.1	−0.09	138.9	179.8	253.7	−0.07	136.5	175.1	249.1	−0.08
PBLH (m)	NARR (land)	872.6	544.1	−37.6	37.6	0.32	556.4	−36.2	36.2	0.40	553.4	−36.6	36.6	0.42	557.1	−36.2	36.2	0.41
	NARR (ocean)	530.0	531.3	0.2	20.6	0.24	615.9	16.2	26.0	0.24	614.7	16.0	25.8	0.25	513.4	−3.1	22.0	0.12
SST (°C)	OAflux (ocean)	28.3	28.5	0.6	1.2	0.76	28.5	0.6	1.2	0.76	28.4	0.4	1.2	0.76	27.5	−2.8	3.8	0.63
	NDBC	27.8	27.9	0.3	1.8	0.96	27.9	0.3	1.8	0.96	27.8	0.2	2.4	0.93	27.0	−2.9	4.8	0.78
LHFLX ($W m^{-2}$)	OAflux (ocean)	111.6	177.8	59.3	59.3	0.61	178.7	60.1	60.2	0.72	179.4	60.7	60.8	0.71	132.7	18.9	26.9	0.47
SHFLX ($W m^{-2}$)	OAflux (ocean)	5.2	15.2	195.4	196.6	0.62	12.3	138.2	139.8	0.67	12.4	140.7	142.4	0.66	7.7	50.2	76.9	0.36

GMDD
8, 9965–10009, 2015

Table 3. Continued.

(b) Species/ Variables	Datasets	obs	BASE				SEN1				SEN2				SEN3			
			sim	NMB (%)	NME (%)	Corr	sim	NMB (%)	NME (%)	Corr	sim	NMB (%)	NME (%)	Corr	sim	NMB (%)	NME (%)	Corr
CO	SEARCH	160	213	33.2	48.7	0.31	241.1	50.6	62.1	0.31	242.5	51.4	63.2	0.30	248.6	49.0	60.2	0.33
SO_2	CASTNET	1.2	3.3	181.8	199.2	0.36	3.6	204.5	219.4	0.31	3.6	201.1	205.6	0.33	3.4	192.1	207.1	0.33
	SEARCH	1.1	0.6	−43.7	97.1	0.06	0.8	−23.0	101.9	0.08	0.9	−21.3	103.0	0.08	0.8	−23.8	102.5	0.06
NO_2	SEARCH	4.2	4.3	1.4	92.7	0.41	5.3	23.6	100.9	0.45	5.4	26.9	104.6	0.43	5.2	23.4	100.1	0.45
HNO_3	CASTNET	1.1	2.0	81.0	82.3	0.70	2.1	92.4	93.0	0.58	2.1	91.9	92.5	0.57	2.0	85.1	85.6	0.62
Max 1 h O_3	CASTNET	51.6	52.5	1.8	19.9	0.52	53.1	3.0	19.4	0.55	52.8	2.4	20.0	0.53	52.6	2.1	19.7	0.54
	AIRS-AQS	52.4	59.5	13.6	23.3	0.58	60.6	15.6	24.2	0.57	60.5	15.4	23.5	0.57	60.2	14.8	23.7	0.58
Max 8 h O_3	CASTNET	46.8	52.3	11.6	21.4	0.58	53.0	13.2	21.5	0.61	52.8	12.7	21.8	0.59	52.5	12.2	21.5	0.59
	AIRS-AQS	47.3	55.6	17.4	24.0	0.99	56.8	20.0	25.5	0.99	56.7	19.8	25.7	0.99	56.6	19.2	25.1	0.99
Hourly O_3	AIRS-AQS	31.7	39.8	25.5	40.2	0.68	40.3	27.3	41.4	0.68	40.2	27.1	41.4	0.68	40.0	26.4	40.7	0.69
	SEARCH	28.3	35.8	26.4	42.0	0.67	37.6	32.7	46.7	0.66	37.5	32.5	46.6	0.66	37.6	32.9	47.0	0.66
NH_4^+	STN	1.0	1.2	19.5	64.4	0.44	1.2	19.6	62.3	0.45	1.2	20.0	63.3	0.44	1.2	17.0	63.0	0.46
	CASTNET	1.2	1.2	−1.4	37.0	0.49	1.2	1.3	35.2	0.50	1.2	0.4	35.1	0.47	1.2	−1.6	34.0	0.51
SO_4^{2-}	IMPROVE	3.1	2.9	−5.4	57.4	0.35	2.9	−5.1	53.6	0.40	2.9	−5.1	52.3	0.41	2.9	−4.0	50.7	0.41
	STN	3.6	3.4	−4.1	57.1	0.30	3.1	−13.9	51.5	0.38	3.1	−13.7	51.1	0.38	3.1	−13.6	52.3	0.34
	CASTNET	4.1	3.6	−10.9	32.2	0.39	3.4	−15.6	31.1	0.43	3.4	−16.1	32.6	0.39	3.4	−17.2	31.5	0.42
NO_3^-	IMPROVE	0.3	0.4	46.7	122.3	0.34	0.4	63.3	138.8	0.23	0.4	62.3	140.1	0.19	0.4	48.6	124.7	0.31
	STN	0.4	0.6	33.3	106.2	0.28	0.7	61.6	128.3	0.26	0.7	63.5	131.7	0.21	0.6	51.0	120.7	0.22
	CASTNET	0.4	0.6	38.7	122.0	0.10	0.6	50.9	130.8	0.10	0.6	48.5	129.3	0.11	0.6	42.4	124.4	0.13
Na^+	IMPROVE	0.4	0.1	−64.6	71.1	0.40	0.1	−68.8	73.8	0.39	0.1	−69.2	73.9	0.39	0.1	−69.0	73.4	0.40
Cl^-	IMPROVE	0.2	0.03	−77.6	82.9	0.52	0.02	−86.0	88.0	0.57	0.02	−85.2	88.2	0.57	0.03	−83.7	85.4	0.66
EC	IMPROVE	0.3	0.3	18.0	63.8	0.45	0.4	43.0	81.1	0.29	0.4	42.2	80.6	0.28	0.4	40.4	79.1	0.27
	SEARCH	1.4	0.4	−71.2	79.4	0.42	0.5	−63.1	75.9	0.48	0.5	−62.2	75.8	0.47	0.5	−63.3	75.8	0.49
OC	IMPROVE	1.5	1.4	−2.5	54.3	0.41	1.9	30.0	66.4	0.40	1.9	28.9	66.0	0.38	1.9	30.3	63.2	0.41
	SEARCH	3.0	1.7	−44.1	59.4	0.25	3.0	−0.4	67.7	0.15	3.0	0.5	68.6	0.15	3.0	−0.4	65.6	0.16
TC	STN	2.9	2.4	−16.2	46.3	0.50	2.9	1.0	46.3	0.46	2.9	1.2	47.5	0.45	2.8	−2.6	46.1	0.45
	SEARCH	3.7	2.3	−40.3	55.4	0.31	3.8	1.5	61.5	0.21	3.8	3.8	63.2	0.21	3.7	0.4	58.9	0.25
$PM_{2.5}$	IMPROVE	10.2	7.9	−22.2	44.7	0.30	9.0	−12.0	40.5	0.31	9.0	−12.0	40.3	0.31	9.0	−11.8	39.0	0.33
	STN	14.1	10.0	−29.3	42.2	0.38	10.6	−25.1	41.5	0.36	10.6	−25.0	41.3	0.36	10.3	−27.1	41.8	0.36
	SEARCH	8.6	7.3	−14.3	80.2	−0.09	10.2	19.1	91.8	−0.06	10.4	21.8	93.0	−0.06	10.3	20.6	89.8	−0.08
PM_{10}	AIRS-AQS	27.4	9.5	−65.4	69.9	0.11	10.4	−62.1	66.8	0.13	10.4	−62.0	66.5	0.14	10.5	−61.7	66.3	0.13

GMDD
8, 9965–10009, 2015

Table 3. Continued.

(b) Species/ Variables	Datasets	obs	BASE				SEN1				SEN2				SEN3			
			sim	NMB (%)	NME (%)	Corr	sim	NMB (%)	NME (%)	Corr	sim	NMB (%)	NME (%)	Corr	sim	NMB (%)	NME (%)	Corr
Col.CO	MOPITT	1.8 $\times 10^{18}$	2.6 $\times 10^{18}$	50.2	50.2	0.78	2.6 $\times 10^{18}$	50.7	50.7	0.81	2.6 $\times 10^{18}$	50.8	50.8	0.80	2.6 $\times 10^{18}$	50.8	50.8	0.80
Col.NO_2	SCIMACHY	1.3 $\times 10^{15}$	2.8 $\times 10^{15}$	116.3	116.7	0.79	3.0 $\times 10^{15}$	129.0	129.2	0.79	3.0 $\times 10^{15}$	129.0	129.3	0.79	3.0 $\times 10^{15}$	132.2	132.4	0.78
Col. SO_2	SCIMACHY	0.27	0.09	−66.6	73.9	0.31	0.10	−61.2	69.7	0.33	0.10	−61.4	69.8	0.33	0.10	−61.1	69.3	0.33
TOR	SCIMACHY	40.1	44.7	11.6	13.0	0.68	46.3	15.6	16.4	0.64	46.4	15.8	16.6	0.64	47.1	17.5	17.8	0.64

The units for all surface gaseous and aerosol species are $\mu g\,m^{-3}$ except for CO (ppb), SO_2 (ppb), NO_2 (ppb) against SEARCH, and O_3 (ppb). The units for column CO and NO_2 are molecules cm^{-2} and for column SO_2 and TOR are DU.

GMDD
8, 9965–10009, 2015

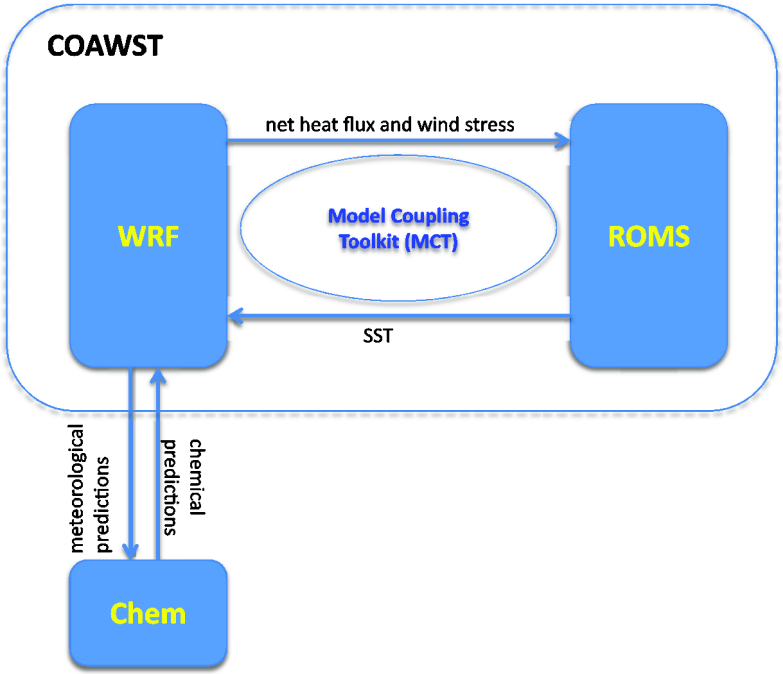

Figure 1. Diagram of WRF/Chem-ROMS coupling within COAWST. The net heat flux and wind stress are passed from WRF to ROMS. The sea surface temperature (SST) is passed from ROMS to WRF. WRF passes predictions of meteorology to its chemistry package. Chemical predictions are passed from the chemistry package to WRF. The two-way coupling between WRF/Chem allows the simulation of feedbacks between chemistry/aerosol and meteorological variables. The two-way coupling between WRF and ROM allows dynamic interactions between atmosphere and ocean.

GMDD
8, 9965–10009, 2015

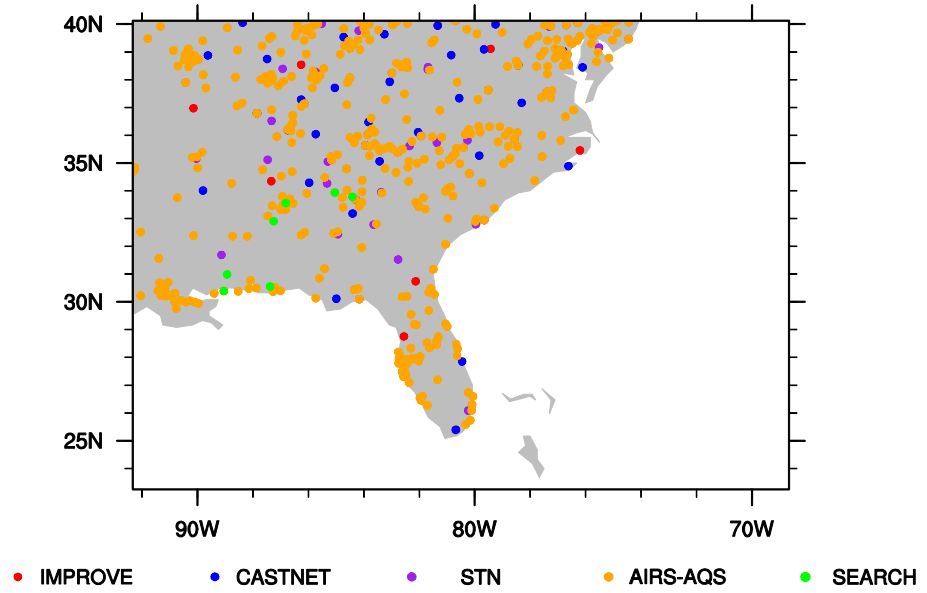

Figure 2. Chemical observational sites including IMPROVE, CASTNET, STN, AIRS-AQS, and SEARCH in the study domain.

GMDD
8, 9965–10009, 2015

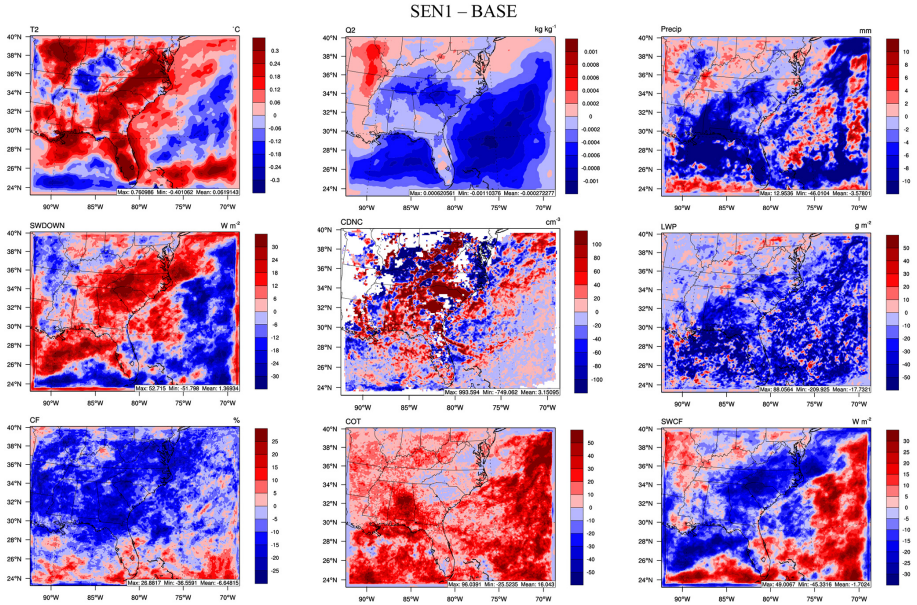

Figure 3.

GMDD
8, 9965–10009, 2015

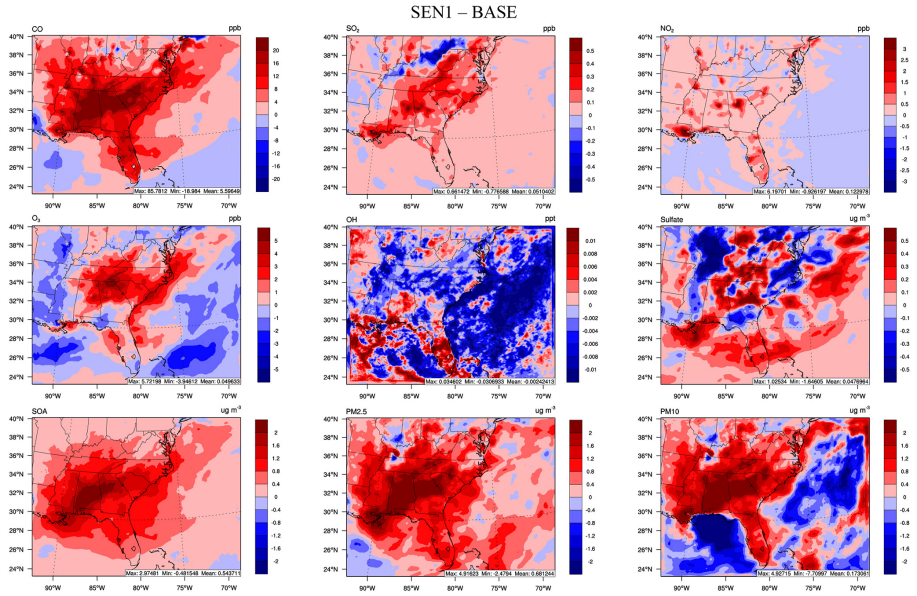

Figure 3. (a) Absolute differences in the predictions of major meteorological and cloud/radiative variables between SEN1 and BASE. **(b)** Absolute differences in the predictions of surface concentrations of chemical species between SEN1 and BASE.

GMDD
8, 9965–10009, 2015

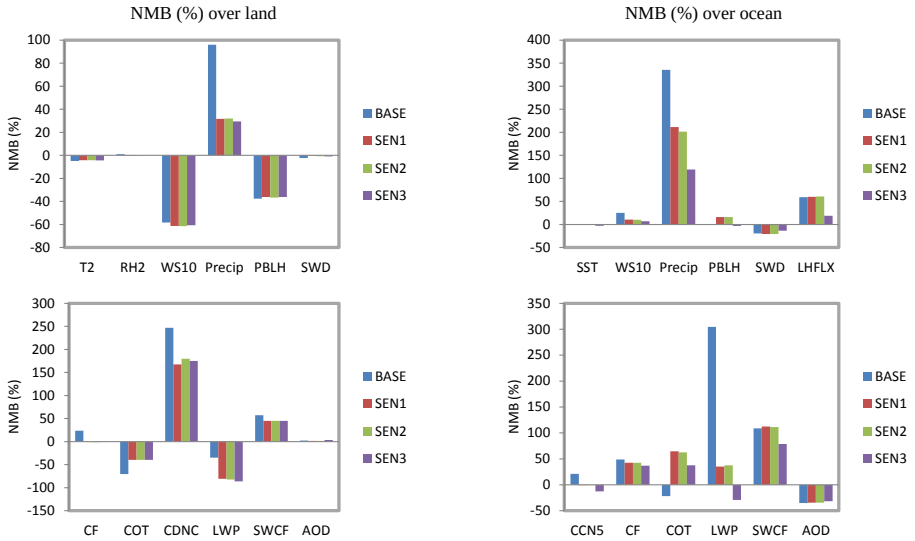

Figure 4. Bar plots of normalized mean bias (NMB, %) for major meteorological, and cloud/radiative variables over land and ocean.

GMDD
8, 9965–10009, 2015

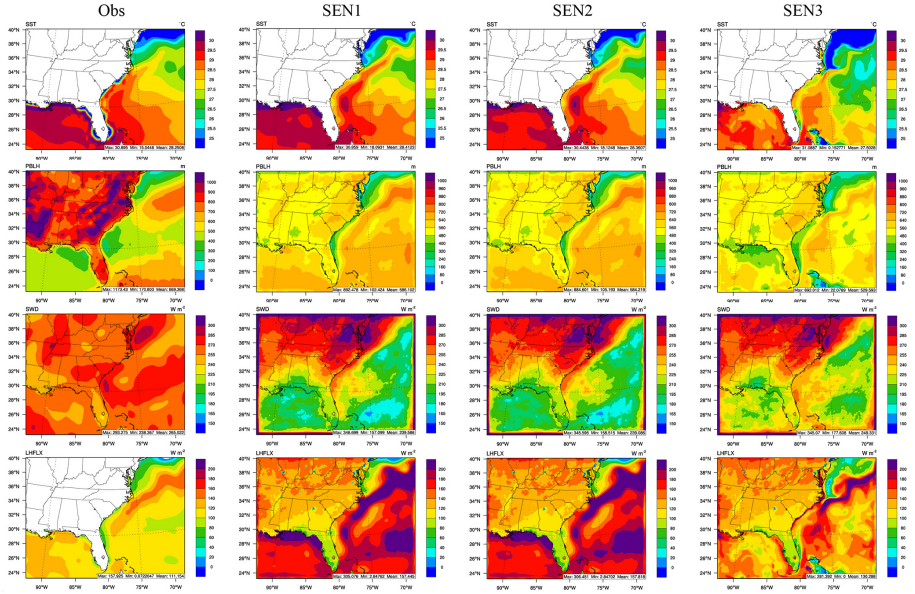

Figure 5.

GMDD
8, 9965–10009, 2015

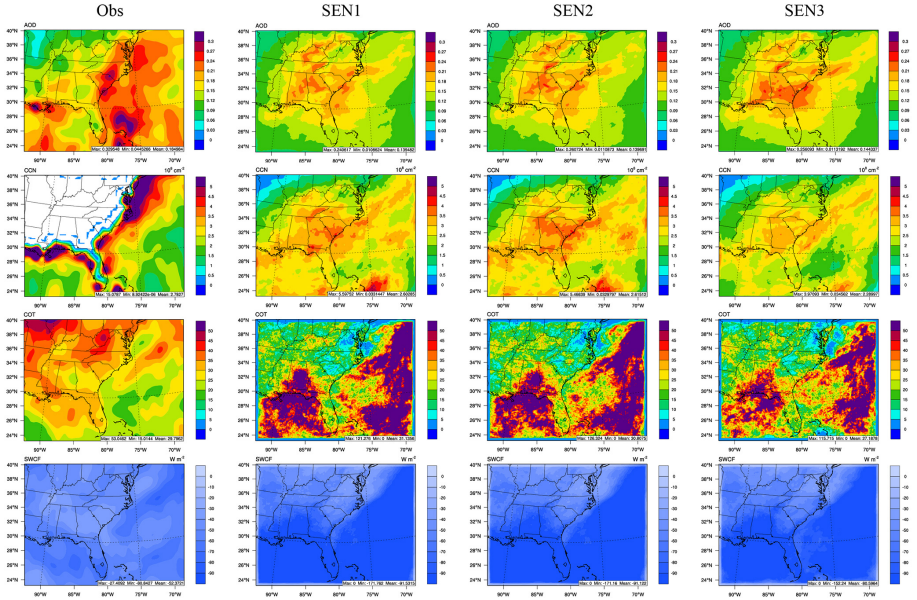

Figure 5. (a) Comparison of satellite retrievals/reanalysis data with the predictions of SST, PBLH, SWD, and LHFLX by SEN1, SEN2, and SEN3. **(b)** Comparison of satellite retrievals with the predictions of for AOD, CCN5, COT, and SWCF by SEN1, SEN2, and SEN3.

GMDD
8, 9965–10009, 2015

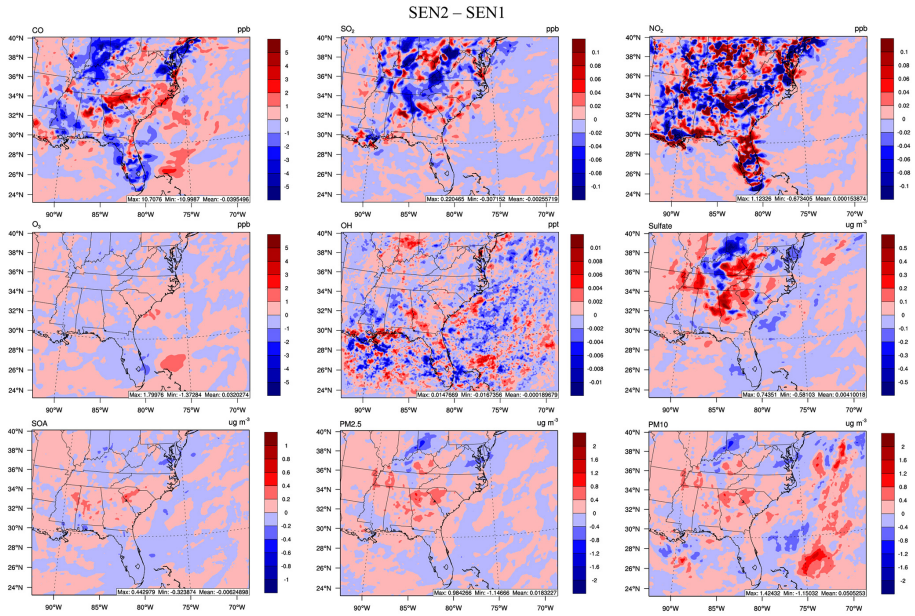

Figure 6.

GMDD
8, 9965–10009, 2015

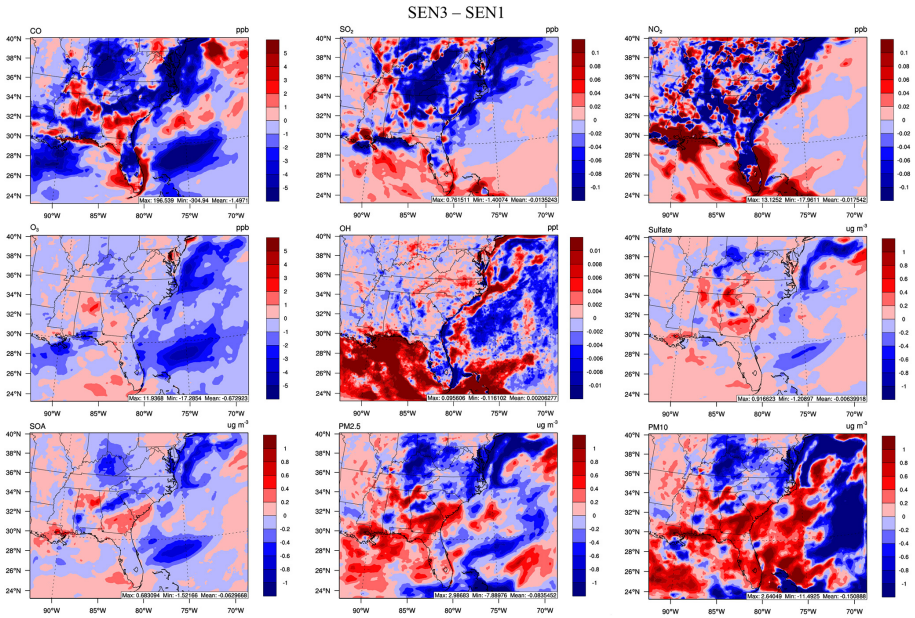

Figure 6. (a) Absolute differences in the predictions of surface concentrations of chemical species between SEN2 and SEN1.**(b)** Absolute differences in the predictions of surface concentrations of chemical species between SEN3 and SEN1.

GMDD
8, 9965–10009, 2015

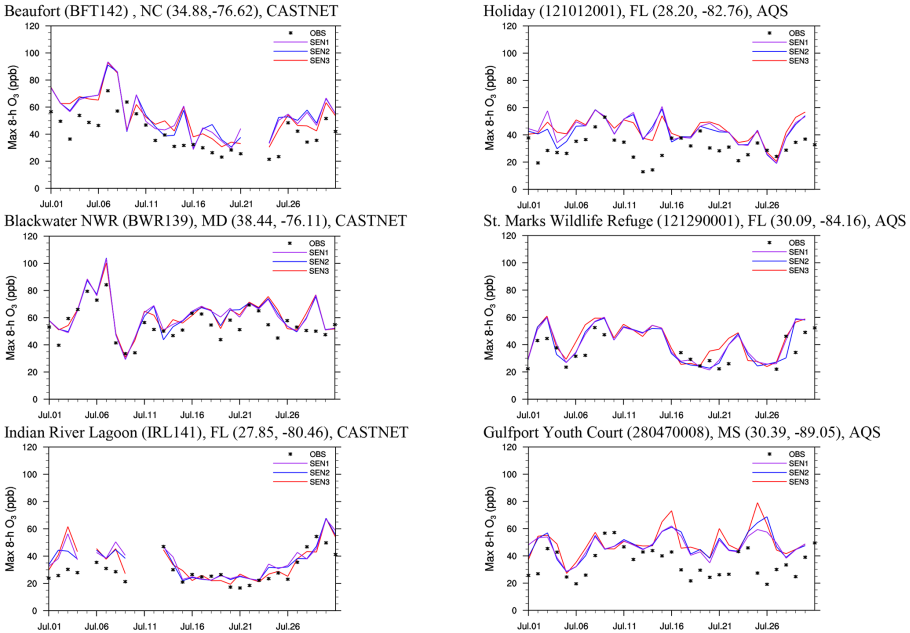

Figure 7.

GMDD
8, 9965–10009, 2015

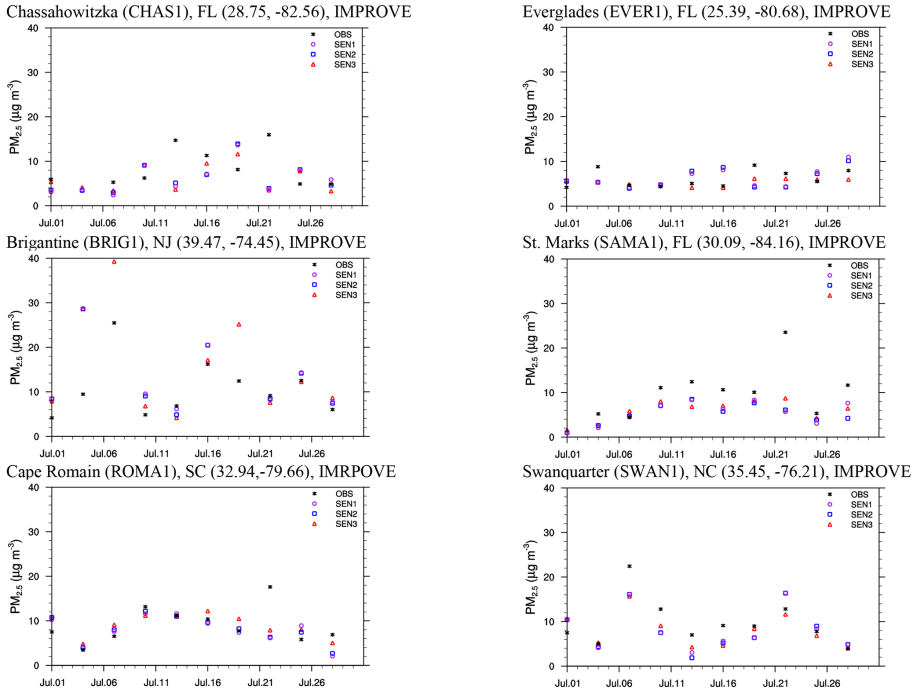

Figure 7. (a) Maximum 8 h ozone at 6 sites, including 3 from CASTNET, and 3 from AIRS-AQS. The black markers represent observations. The purple, blue, and red lines represent simulated results from SEN1, SEN2, and SEN3, respectively. **(b)** Surface $PM_{2.5}$ concentrations at 6 sites from IMRPOVE. The black markers represent observations. The purple, blue, and red markers represent simulated results from SEN1, SEN2, and SEN3, respectively.

GMDD
8, 9965–10009, 2015

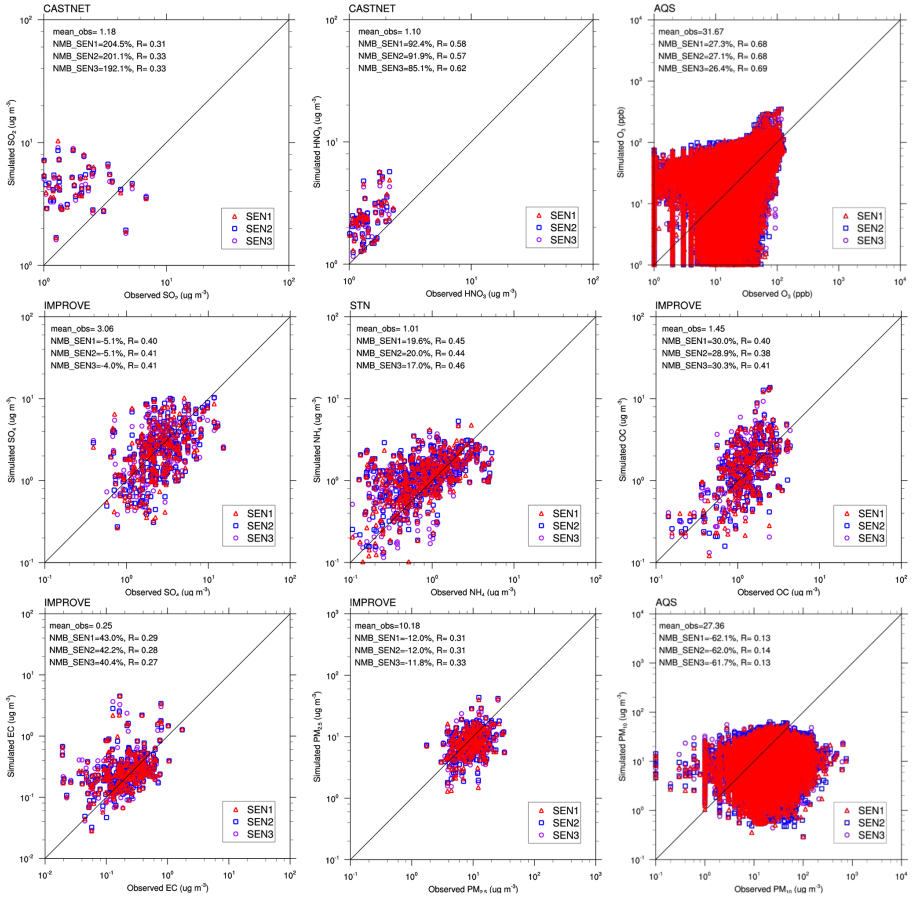

Figure 8. Scatter plots of simulated vs. observed concentrations of major chemical species over different networks.

GMDD
8, 9965–10009, 2015